Mine Water and the Environment (2022) 41:1015–1026
https://doi.org/10.1007/s10230-022-00895-2

TECHNICAL ARTICLE

Hydrogeochemical Characteristics and Formation Mechanisms of the Geothermal Water in the Qingdong Coal Mine, Northern Anhui Province, China

Jiying Xu[1,2,3] · Herong Gui[3] · Jiayu Chen[4] · Chen Li[4] · Ye Li[5] · Chengzhou Zhao[5] · Yan Guo[3]

Received: 1 March 2021 / Accepted: 25 July 2022 / Published online: 1 August 2022

Abstract

The hydrogeochemistry of geothermal fluids provides insight into the occurrence, formation, and circulation of geothermal resources. We collected 13 geothermal water (> 34 °C) and 11 common groundwater samples (< 20 °C) from the Qingdong coal mine in China. The geothermal water samples had higher TDS, Ca^{2+}, and SO_4^{2-} contents, by 1.22-, 1.28-, and 1.25-fold, respectively. The hydrochemical facies of the geothermal water samples was 92% SO_4·Cl–Ca.Mg and 8% SO_4·Cl–Na, whereas the common groundwater samples was 73% SO_4·Cl–Ca.Mg and 27% SO_4·Cl–Na. Moreover, hydrogen and oxygen isotopic analysis revealed that atmospheric precipitation and water–rock interaction were the sources of the geothermal water. The chemical composition of the geothermal water is dominated by ion-exchange interactions and the dissolution of carbonates and silicates. Overall, geothermal water in the study area is characterized by optimal hydrodynamic conditions and more intense ion-exchange interactions than common groundwater. Moreover, the formation of geothermal water is controlled by hydrogeological and structural conditions, and by the infiltration of atmospheric precipitation, heating by deep circulation, and transportation by water-conducting faults (F_{11}) to shallow coal strata. These results will facilitate the development of geothermal resources and the construction of green ecological mines, which will provide considerable economic and social benefits.

Keywords Hydrochemical characterization · Water–rock interaction · Recharge source · Huaibei coalfield · Stable isotopes

Introduction

Geothermal resources are a type of green energy that forms under unique geological conditions and integrates heat, water, and minerals to form highly valuable resources. Compared with coal, oil, natural gas, and other energy sources, geothermal resources have the advantages of high utilization rates, low costs, and low environmental pollution. Moreover, they can be used in power generation, heating, aquaculture, medical care, and hot spring bathing, with

✉ Herong Gui
guiherong@163.com

Jiying Xu
jiyingxu1986@163.com

Jiayu Chen
nuomituan99303@163.com

Chen Li
lichen960603@163.com

Ye Li
276319529@qq.com

Chengzhou Zhao
405547419@qq.com

Yan Guo
798767854@qq.com

[1] School of Resources and Geoscience, China University of Mining and Technology, Xuzhou 221116, Jiangsu, China

[2] Key Laboratory of Mine Water Resource Utilization of Anhui Higher Education Institutes, Suzhou University, Suzhou 234000, Anhui, China

[3] National Engineering Research Center of Coal Mine Water Hazard Controlling, Suzhou University, Suzhou 234000, Anhui, China

[4] School of Earth and Environment, Anhui University of Science and Technology, Huainan 232001, Anhui, China

[5] Huaibei Mining Co. Ltd, Huaibei 235000, Anhui, China

considerable economic and environmental benefits (Erdogdu 2009; Weiß 2020). Geothermal energy research is currently being conducted in more than 80 countries worldwide (Nasruddin et al. 2016; Darma 2016). China is a country with abundant geothermal resources. Medium -and low-temperature geothermal resources are widespread throughout the country, especially in the North China Basin, which has significant development and utilization potential (Chen et al. 1995; Hou et al. 2018).

The Huaibei coalfield situated to the south of the North China Basin is characterized by abundant coal resources. With the continuous mining over the last few decades, the area has been mined to great depths (Gui et al. 2018). A highly developed fault system in this coalfield facilitates groundwater penetration into deep underground fractures and fissures, where it is heated by high-temperature rock. This water then circulates back to shallower regions under favorable geological conditions, forming abundant geothermal water resources (Gui and Lin 2016).

The hydrochemical components and isotopic characteristics of geothermal fluids often retain detailed geochemical information pertaining to the formation and evolution of the geothermal system, and this can be used to analyze the origin of geothermal fluids, the geological conditions of geothermal formation, and the associated geochemical processes (Chen et al. 2014; Tran et al. 2020). Therefore, the hydrogeochemistry of geothermal fluids is an effective tool for understanding the formation mechanism, occurrence environment, and circulation mechanism of geothermal resources. Numerous studies on the hydrogeochemical characteristics of geothermal water have been conducted to explore geothermal genesis, geothermal water exploitation, the relationship between the chemical components of geothermal water, volcanoes, and earthquakes, and hydrothermal mineralization (Chen et al. 2020; Gu et al. 2017; Karaoğlu et al. 2019; Zhang et al. 2019b). In addition, hydrochemical parameters and isotopes have been used to assess the recharge source and age, classify hydrochemical type, analyze the water–rock balance, and estimate the temperature of the reservoir and the circulation depth of geothermal water (Alçiçek et al. 2019; Chenaker et al. 2018; Xu et al. 2019). Moreover, considerable research has been conducted on the source, quality, and evolution of common groundwater in coal mines; however, little is known about the hydrogeochemical characteristics and formation mechanisms of deep geothermal water in coal mines.

In this study, we aimed to: (1) investigate the differences in chemistry and hydrogeochemical processes of geothermal water and common groundwater in coal mines, and (2) determine the recharge source and formation mechanism of geothermal water. The outcomes of this study will facilitate better understanding of geothermal resources and will aid the construction of green ecological mines.

Methods

Study Area

The Qingdong coal mine is located 45 km from the city of Suzhou in Anhui Province, China. Its geographical coordinates are 116°25′44″–116°34′44″ E and 33°36′34″–33°40′29 N (Fig. 1a, b). The mining area is ≈13 km long (east to west), 3.5–6.5 km wide (north to south) and covers an area of 51.7 km^2. The terrain in the area is relatively flat, with an elevation of + 27.6 to + 31.4 m. The coal mine was developed in June 2007, with a designed production capacity of 1.8 mt/a.

The study area is predominately monsoonal, which entails a warm, temperate, and semi-humid climate with an average annual rainfall of ≈ 811.8 mm, an average wind speed of ≈ 3 m/s, an annual cumulative evaporation of ≈ 1890.6 mm, and an annual average temperature of 14.6 °C. A medium-sized seasonal river, the Huihe River, is situated close to the mine and is characterized by an average annual discharge of 42.1 m^3/s and an average annual water level elevation of 22.7 m.

The coal mine is in a block formed by nearly EW and NNE faults, which belong to a dustpan block type structure. The main structural form is mono-clinic, NW-EW trending, and N dipping. The deposit is covered entirely by Quaternary and Neogene loose layers from the Cenozoic period. The groundwater system can be divided into a Quaternary aquifer (group), a coal-bearing aquifer (group), and a limestone aquifer (group) (Chen and Gui 2017), as shown in supplemental Fig. S1.

Limestone aquifers are commonly observed in coal mines in China and here includes the Taiyuan and Ordovician formations. Characteristics of limestone aquifers such as proximity to the coal seam, high water pressure, and abundant water quantity pose a severe threat to the safety of mining activity. Based on the geological data of the Huaibei coalfield, this aquifer mainly consists of medium-thick layers of carbonate rocks, and is prone to developing a karst collapse column, which can cause serious geological disasters; if a water-conducting fault or collapse column is encountered during tunnel engineering, the water in the limestone aquifer can directly fill the mine or cause a water inrush accident through the tubular channel (Zhang et al. 2019c). Therefore, to mine the no. 10 coal at the bottom of the coal strata, the water pressure of the limestone aquifer water under this coal seam floor must be reduced to 0 MPa. Since the Ordovician limestone water is situated far from the coal seam floor, water in the Taiyuan Formation is typically drained.

To avoid accidents associated with water-conducting faults or collapse columns, boreholes in the Qingdong coal

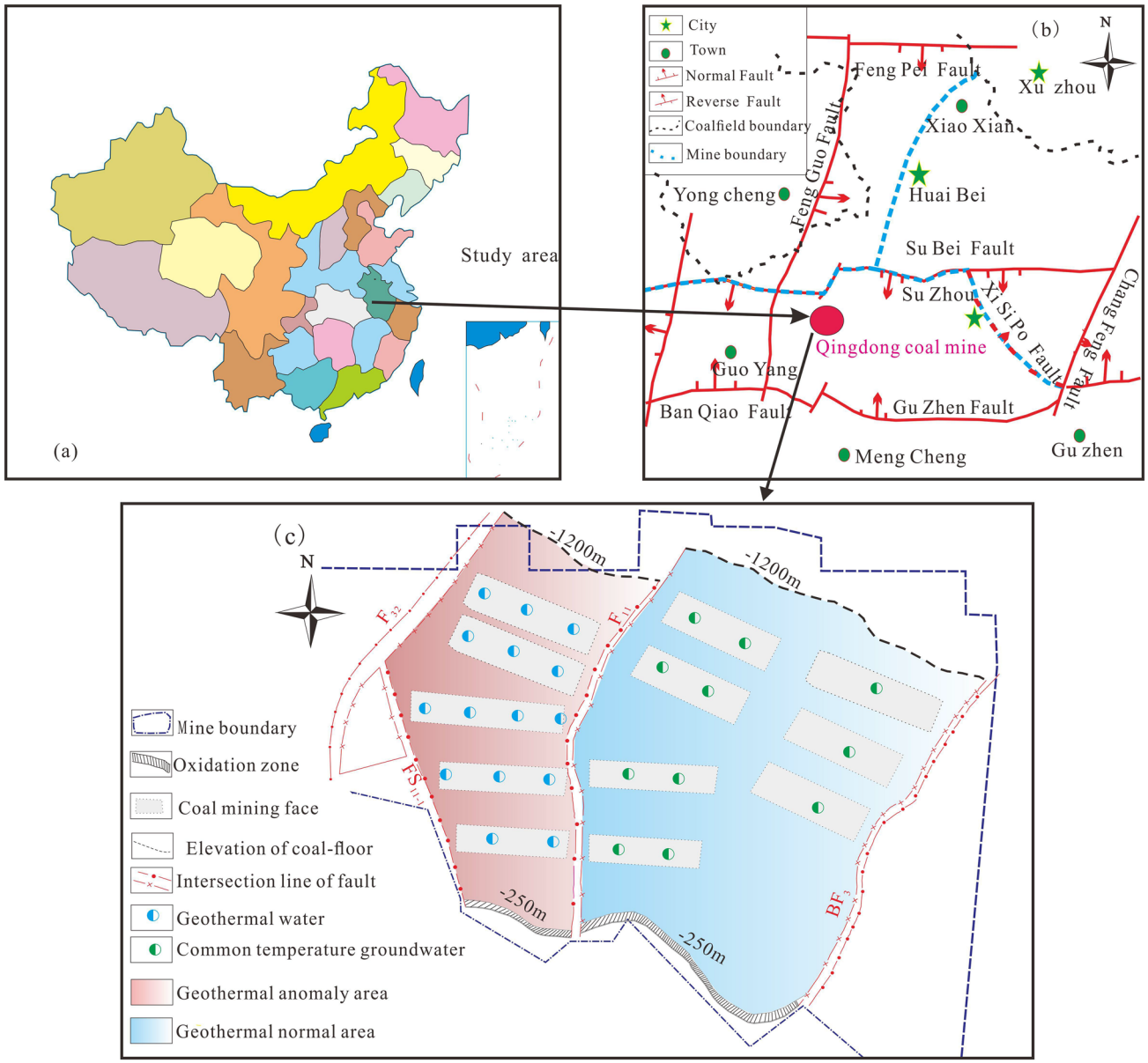

Fig. 1 Geographic location (**a**); Geological map of the study area (**b**) and the location of samples (**c**)

mine were drained from − 585 m to the Taiyuan Formation in the Qingdong coal mine. The characteristics of samples collected near the F_{11} fault (Fig. 1a) showed significant differences. During the drainage process, a geothermal anomaly was detected in the western area of the coal mine, where the water temperature of the groundwater ranged from 34.6 to 41.2 °C, significantly higher than the average groundwater temperature in the east (18 °C). Groundwater temperatures at the same level were also significantly lower than the anomaly. Furthermore, according to the geothermal borehole analysis results, the value of the geothermal gradient in the west area was 3.1 °C/100 m, which is significantly higher than that in the eastern area (2.5 °C/100 m).

Sample Collection and Analysis

To study the hydrogeochemical characteristics and formation mechanisms of geothermal water in the study area, a total of 24 groundwater samples were collected from drainage boreholes (− 585 m) in May 2017, including 13 samples from the geothermal anomaly area (west) and 11 samples from the normal area (east). The locations of the sampling points are shown in Fig. 1c. Samples were collected in pre-cleaned

HDPE bottles. Before sampling, the bottles were rinsed with the sample water three times, after which the collected samples were sealed with sealing film on site. The pH and total soluble solids (TDS) of all the samples were measured using portable devices from OHAUS (Shanghai, China). The samples were filtered using 0.45 μm filter paper within 24 h after collection and stored at low temperatures until analysis.

Compositions of main cations (Na^+, K^+, Ca^{2+}, and Mg^{2+}) and anions (SO_4^{2-}, Cl^-) in the samples were analyzed using an ion chromatograph (ICS-600-900, USA). The contents of CO_3^{2-} and HCO_3^- were determined by acid–base titration (analysis error was controlled within 5%). The stable isotopes of hydrogen and oxygen (δD, $\delta^{18}O$) were measured using an isotope analyzer (LGR-LWIA-45EP, USA). The measurement accuracies of δD and $\delta^{18}O$ were 1.0 ‰ and 0.2 ‰, respectively. Before all samples were tested, the stability of the test instrument was ensured using standard samples, and the relative deviation of parallel samples was less than 5%.

Results and Discussion

Hydrochemical Characterization

The descriptive statistics of hydrochemical characteristics, including major ion concentrations, pH, TDS, and isotopic data were summarized in Table 1. The parameters were comprised of maximum, minimum, mean, standard deviation, coefficient of variation, and a confidence interval of 95%. As shown in supplemental Fig. S2, a box plot with normal curve was performed to compare the characteristics of the two types of groundwater. Based on the actual groundwater temperature, the samples were divided into two groups: geothermal water (> 34 °C) and common groundwater (< 20 °C). As the properties of K^+ are similar to those of Na^+ and the concentration of K^+ in the coal mine groundwater is significantly less than that of Na^+, the concentrations of K^+ and Na^+ were merged (Zhang et al. 2020a).

Overall, the coefficient variation of all the indexes was less than 0.5, indicating that the chemical constituents exhibited a low to medium spatial fluctuation. The TDS values of the geothermal water samples ranged from 2488–3681 mg/L, whereas the TDS of the common groundwater samples displayed a narrower range of 2383–2805 mg/L. The highest TDS content recorded for the geothermal water samples was 1.31-times that of the common groundwater. In addition, all the geothermal water and common groundwater samples recorded TDS values > 1000 mg/L, which exceeds the World Health Organization and China's national drinking water quality guidelines. All geothermal water and common groundwater samples were weakly alkaline, with average pH values of 7.6. This result is consistent with those of previous water analyses in other coal mines in the Huaibei coalfield (Hu et al. 2015; Wang et al. 2019), but greater than that of the Huainan coalfield (Zhang et al. 2019a).

The Piper trigram is a useful for revealing the hydrogeochemical characteristics and evolution processes of water (Karmegam et al. 2011). To compare the hydrogeochemical characteristics between geothermal water and common groundwater, a piper trigram of the samples was plotted (supplemental Fig. S3). The geothermal water and common groundwater samples were mostly concentrated in Zone 6 and rarely in Zone 7, indicating that the content of alkaline earth metal ions was higher than that of alkali metal ions, and the content of strong acid roots was higher than that of weak acid roots. The hydrochemical facies of the common groundwater samples were dominated by SO_4·Cl–Ca.Mg (73%) and SO_4·Cl–Na (27%). With the increase in Ca^{2+} content and decrease in $Na^+ + K^+$, the hydrochemical facies of the geothermal water samples changed to 92% SO_4·Cl–Ca·Mg and 8% SO_4·Cl–Na, resulting in left and downward shifting of the data points in the ternary cation diagram. For cations, the geothermal water samples mostly

Table 1 Hydrochemical data of samples

Types	pH	$Na^+ + K^+$ mg/L	Ca^{2+}	Mg^{2+}	Cl^-	SO_4^{2-}	HCO_3^-	TDS	δ (D) ‰	δ (^{18}D)
Geothermal water > 34 °C										
Min	6.9	81.19	195.6	53.20	204.2	1397	207.7	2488	− 9.2	− 73.7
Max	8.1	566.0	710.6	211.7	335.0	2089	297.7	3681	− 8.2	− 69.7
Mean	7.6	331.8	466.6	133.1	249.6	1785	242.0	3082	− 8.8	− 71.0
CV	5.5%	39.8%	35.4%	35.0%	13.5%	12.9%	9.2%	11.7%	4.2%	2.0%
Common groundwater < 20 °C										
Min	7.13	243.0	243.0	199.4	30.95	1271	188.3	2383	− 8.7	− 68.2
Max	8.50	518.9	518.9	495.3	192.9	1594	291.4	2805	− 8.2	− 65.1
Mean	7.62	362.8	362.8	281.8	123.3	1425	266.4	2518	− 8.4	− 67.0
SD	0.38	93.85	93.85	83.40	43.00	93.90	30.52	134.8	0.23	1.08
CV	5.0%	25.9%	25.9%	29.6%	34.9%	6.6%	11.5%	5.4%	− 2.7%	− 1.6%

plotted in zone A (calcium type) and in zone B (mixed type), whereas the common groundwater samples plotted in zones B and D. The phenomenon of high Ca^{2+} content and low $Na^+ + K^+$ content in the geothermal water samples was not consistent with the characteristics of coal mine water in the Huaibei coalfield. For anions, all the samples plotted in zone F, which is dominated by SO_4^{2-}, implying that sulfate mineral dissolution plays an important role during the hydrogeochemical process. In general, the hydrochemical facies of the geothermal water samples were more complex and diverse than those of the common groundwater samples.

Hydrogeochemical Process

Water–Rock Interactions

Water–rock interactions significantly influence the chemical composition of groundwater. Moreover, analyzing the ratio of anions and cations can reveal the source of the main ions and provide insights into geochemical processes (Hao et al. 2021).

If halite was the only dissolved mineral in water, the molar ratio between Na^+ and Cl^- in groundwater should be 1:1 (Guo et al. 2020). As shown in Fig. 2a, all the data points of the geothermal water and common groundwater samples plotted below the NaCl dissolution line, indicating that Na^+ in the water samples was not exclusively sourced from halite. Compared with the geothermal water samples, the common groundwater samples had higher Na^+ concentrations, suggesting a relation to the abundant albite (Eq. 1) in the coal measure strata.

$$\begin{aligned} &Na_2Al_2Si_6O_{16}(\text{albite}) + 2CO_2 + 3H_2O \\ &\rightarrow 2HCO_3^- + 2Na^+ + H_4Al_2SiO_9 + 4SiO_2 \end{aligned} \quad (1)$$

If gypsum was the only dissolved mineral, the molar ratio between $Ca^{2+} + Mg^{2+}$ and SO_4^{2-} in groundwater should be 1:1 (Liu et al. 2020a). As shown in Fig. 2b, all the data points of the geothermal water and common groundwater samples plotted above the $Ca_xMg_{1-x}SO_4$ dissolution line, indicating the existence of other SO_4^{2-} sources. Moreover, the excess SO_4^{2-} in the samples was likely related to abundant pyrite (Eq. 2) in the coal mine strata.

$$2FeS_2(\text{pyrite}) + 7O_2 + 2H_2O \rightarrow 2FeSO_4 + 4H^+ + 2SO_4^2 \quad (2)$$

If the molar ratio between $Ca^{2+} + Mg^{2+}$ and $HCO_3^- + SO_4^{2-}$ in groundwater is equal to 1:1, this indicates that the Ca^{2+} and Mg^{2+} in the water were derived from dissolution of carbonate minerals (calcite, dolomite, and gypsum) (Chen et al. 2017; Chen and Sun 2019). As shown in Fig. 2c, the data points of the common groundwater samples plotted around the 1:1 dissolution line, indicating that carbonate dissolution was the main source of Ca^{2+} and Mg^{2+} in the samples. In contrast, all the geothermal samples plotted above the 1:1 dissolution line, suggesting excess $HCO_3^- + SO_4^{2-}$ in the geothermal water. This suggests that the composition of $Ca^{2+}$and Mg^{2+} in the geothermal water samples is controlled by both carbonate and silicate dissolution.

The molar ratio between Ca^{2+} and Mg^{2+} is referred to as the calcium magnesium coefficient; a large coefficient implies a longer groundwater storage time and stronger degree of water–rock interaction (Zhang et al. 2020b). As shown in Fig. 2d, the data points of the common groundwater samples plotted in the lower left section of the 1:1 dissolution line and the coefficient was slightly greater than 1. Conversely, the geothermal water samples plotted in the lower right section of the 1:1 dissolution line and the coefficient was close to 3. These results suggest that water–rock interactions had influenced the geothermal water more than the common groundwater.

The relationship between Cl^-/Ca^{2+} and Cl^- can reveal the hydrodynamic conditions of groundwater (Hao et al. 2020). An inverse relationship between Cl^-/Ca^{2+} and Cl^- indicates that the groundwater has fine hydrodynamic conditions and experiences sufficient leaching. The slopes of the linear fitting lines of the common groundwater and geothermal water samples were 0.077 and − 0.039, respectively (Fig. 2e). This indicates that the runoff of the common groundwater samples is relatively slow, whereas geothermal water possesses fine hydrodynamic conditions and strong water–rock interactions.

Dissolution/ Weathering Process

Plots of Mg^{2+}/Na^+ and HCO_3^-/Na^+ vs. Ca^{2+}/Na^+ are commonly used to assess if evaporation, silicate weathering, and carbonate dissolution are involved in water–rock interactions (Guan et al. 2020). The data points of the samples plotted between the carbonate and the silicate dominance zones but far from the evaporation dominance zone, indicating that silicate weathering and carbonate dissolution were the main water–rock interaction processes in the study area. The data points of the geothermal water samples plotted closer to the carbonate dominance zone than the common groundwater samples (Fig. 3), suggesting that these geothermal samples contained more dissolved carbonate minerals.

The Gibbs ratios, $Na^+/(Na^+ + K^+)$ vs. TDS, and $Cl^-/(Cl^- + HCO_3^-)$ vs. TDS can be used to determine the dominant factors influencing the chemical composition of water, including precipitation, rock dissolution, and evaporation (Oosawa and Kasai 1988). The data points of all of the samples plotted between the rock dominance and evaporation dominance zones, but far from the precipitation

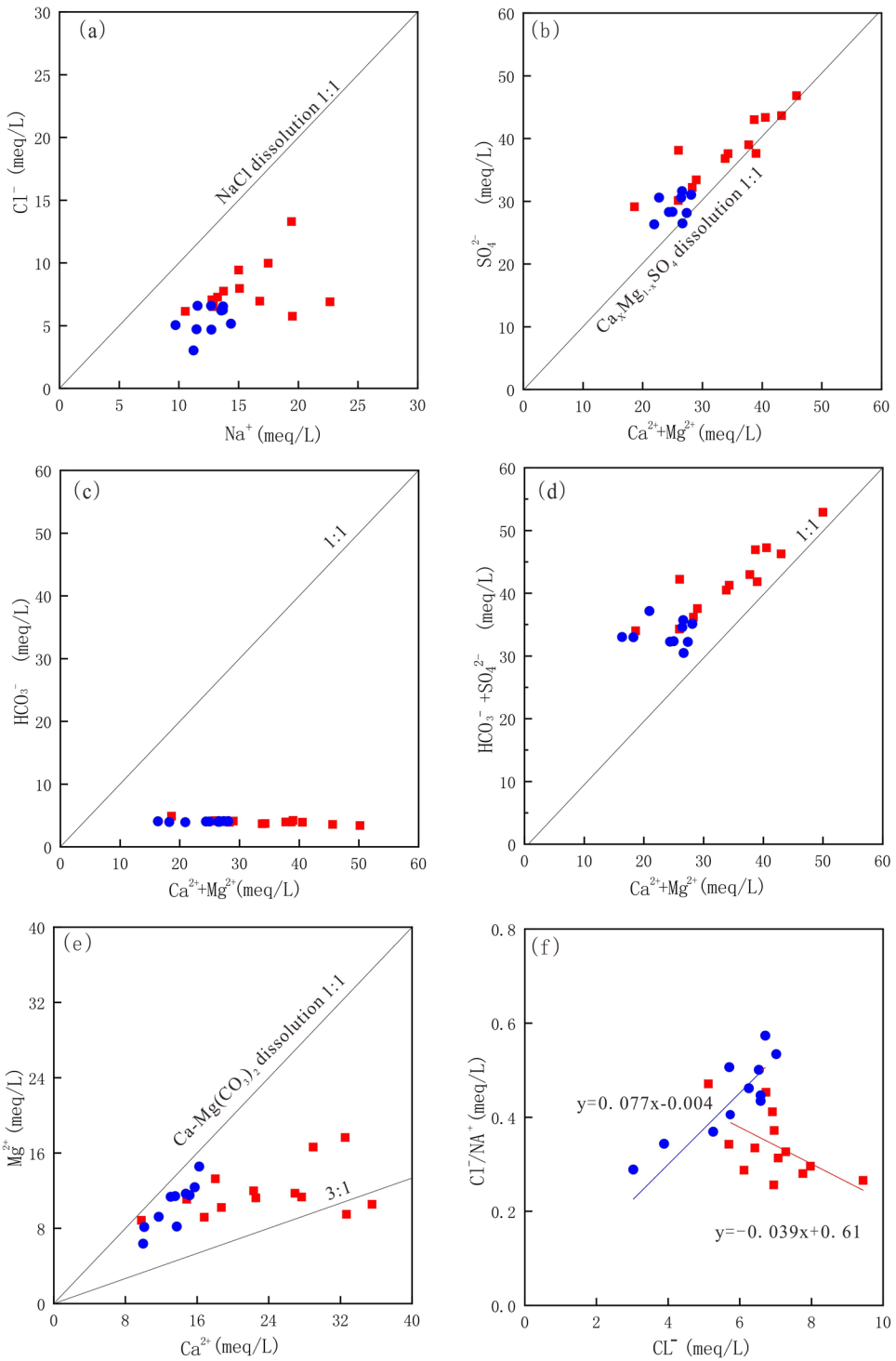

Fig. 2 Plots of **a** Cl^- versus Na^+; **b** SO_4^{2-} versus $Ca^{2+}+Mg^{2+}$; **c** $(HCO_3^- + SO_4^{2-})$ versus $(Ca^{2+}+Mg^{2+})$; **d** Mg^{2+} versus Ca^{2+}; **e** Cl^-/Ca^{2+} versus Cl^-

dominance zone, indicating that the chemical composition of the samples was controlled by rock weathering and evaporation. Compared with the common groundwater samples, the data points of the geothermal water samples plotted in the left section of the diagram (Fig. 4a) indicating that the geothermal water was characterized by a lower concentration of $Na^+ + K^+$ and a higher concentration of TDS.

Ion-Exchange Interaction

Ion exchange is an important process for controlling the chemical composition of groundwater. A bivariate plot

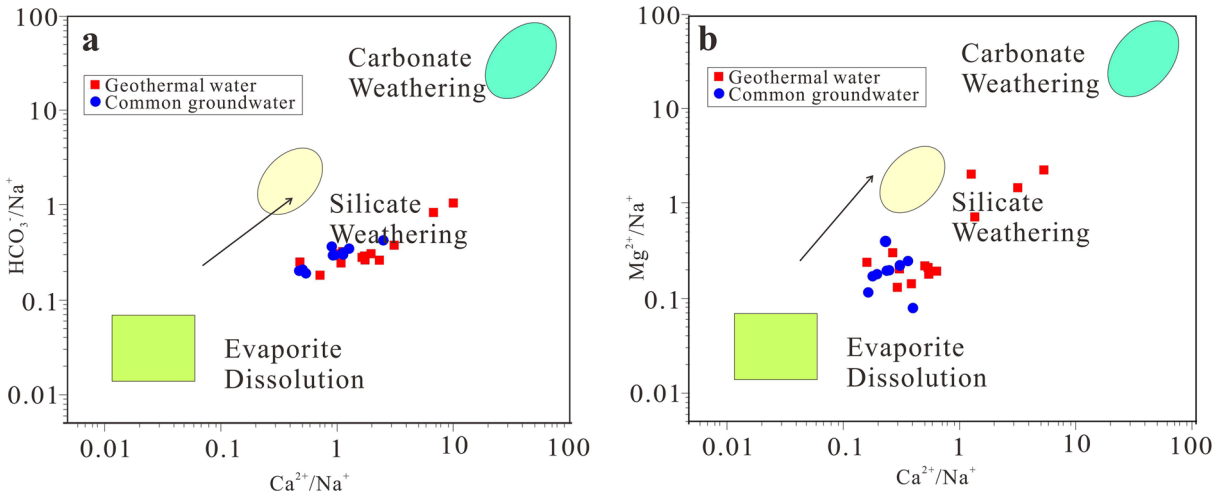

Fig. 3 The relationship between HCO_3^-/Na^+ and Ca^{2+}/Na^+ (**a**) and between Mg^{2+}/Na^+ and Ca^{2+}/Na^+ (**b**)

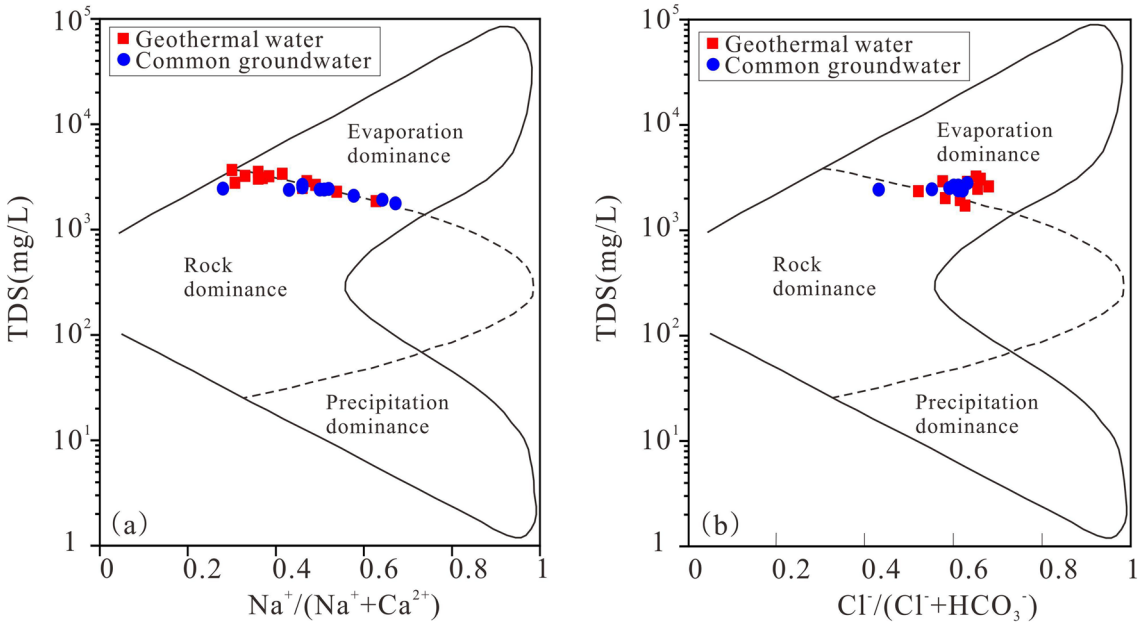

Fig. 4 Gibb's diagram of geothermal water and common groundwater. **a** cationic; **b** anionic

$(Ca^{2+} + Mg^{2+}–SO_4^{2-}–HCO_3^-$ vs. $Na^+ + K^+–Cl^-)$ was analyzed to determine if points on the diagram plot near a straight line with a slope of − 1, which would indicate the presence of cation exchange in the groundwater (Kim et al. 2004; Wang et al. 2015). As shown in Fig. 5a, the data points of the geothermal water samples plotted on a straight line with a slope of − 1.04 and an R^2 value of 0.93, whereas the data points of the common groundwater samples plotted along a line with a slope of − 1.27 and an R^2 value of 0.76. These results suggest that, apart from dissolution, ion-exchange interactions influence the chemical compositions of groundwater in the study area. Moreover, the high R^2 value (0.93) of geothermal water in the bivariate plot suggests that ion-exchange interactions are the primary factors influencing chemical composition. Conversely, the low R^2 value (0.76) of the common groundwater samples indicates that ion-exchange interactions do not significantly affect that water's chemical composition.

The ion exchange interactions can also be analyzed by choro-alkaline indices. Two indices, CA-1 and CA-2, were calculated for the water samples using Eqs. (3) and (4):

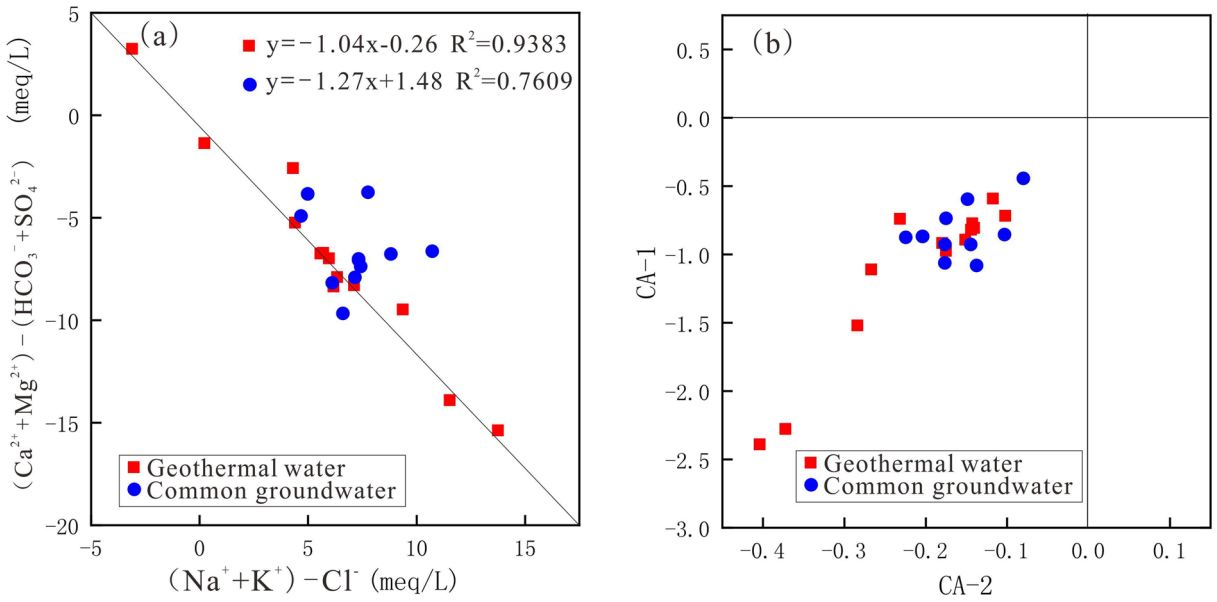

Fig. 5 The relation between ($Ca^{2+}+Mg^{2+}$-SO_4^{2-}-HCO_3^-) and ($Na^+ + K^+$-Cl^-) (**a**) and CA-1 and CA-2 (**b**)

$$CA-1=\left[Cl^- - \left(Na^+ + K^+\right)/Cl\right] \tag{3}$$

$$CA-2=\left[Cl^- - \left(Na^+ + K^+\right)\right]/\left[HCO_3^- + SO_4^{2-} + CO_3^{2-} + NO_3^-\right] \tag{4}$$

Positive values of CA-1 and CA-2 suggest that Na^+ and K^+ in the groundwater have been exchanged by Ca^{2+} and Mg^{2+} in the surrounding rock, whereas negative values indicate the reverse. In addition, larger absolute values indicate stronger ion-exchange interactions. Moreover, a value of 0 indicates no ion exchange interaction during the hydrochemical process (Keesari et al. 2021; Tay et al. 2014). Figure 5b shows the plot of CA-1 vs. CA-2 for the geothermal water and common groundwater samples. The data points of all of the samples plotted in the negative section of the diagram, indicating that Ca^{2+} and Mg^{2+} in the water had been replaced by Na^+ and K^+ from the host rock.

$$2Na^+(\text{rock}) + Ca^{2+}(\text{groundwater}) \rightarrow 2Na^+(\text{groundwater}) + Ca^{2+}(\text{rock}) \tag{5}$$

The results showed that the CA-1 and CA-2 values of the common groundwater samples ranged from − 0.38 to 1.32 and − 0.08 to − 0.22, respectively. In the geothermal water samples, the CA-1 values ranged from − 0.52 to − 2.48, and the CA-2 values ranged from − 0.14 to − 0.42. Therefore, the geothermal water in the study area is characterized by higher absolute values of CA-1 and CA-2 than the common groundwater, suggesting that ion-exchange interactions are more prevalent in the geothermal water.

Recharging Analysis

Analyzing the isotopic composition of groundwater provides insights into the recharge sources. δD and $\delta^{18}O$ are ideal tracers of water recharge within different flow systems (Prada et al. 2016). During the water circulation process, due to the equilibrium and thermal fractionation of isotopic composition, a linear relationship exists between the stable isotopes of δD and $\delta^{18}O$ in global precipitation, which is expressed as $\delta D = 8\,\delta^{18}O + 10$ and was defined as the global meteoric water line (GMWL) by Craig (1961). If water samples plot near the GMWL, this indicates an atmospheric precipitation recharge source.

The values of δD and $\delta^{18}O$ described in the δD-$\delta^{18}O$ coordinate system composed of the GMWL and the regional local evaporation line (LEL) (Chen et al. 2010; Liu et al. 2009), as shown in Fig. 6. Hydrogen and oxygen isotope data were obtained from various aquifers in the Huaibei coalfield, including deep and shallow aquifers, surface water, and the Quaternary and limestone aquifers (Taiyuan and Ordovician formations) (Gui et al. 2005; Gui and Chen 2016). Meanwhile, the δD and $\delta^{18}O$ compositions of the geothermal (n = 6) and common (n = 5) groundwater samples were plotted on a δD-$\delta^{18}O$ relationship diagram.

All of the water sample data points plotted in the lower part of the GMWL and LEL (Fig. 6), suggesting that they originated from precipitation and experienced varying degrees of evaporation during the recharging process. Overall, the δD and $\delta^{18}O$ compositions of the aquifers in the Huaibei coalfield decreased from shallow to deep, showing a trend toward the lower left corner. The $\delta^{18}O$ for

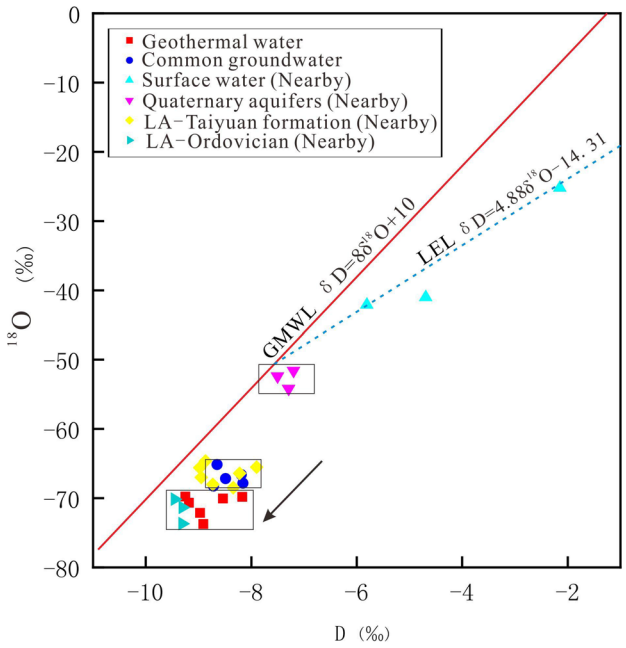

Fig. 6 The plot of $\delta^{18}O$ versus δD

the geothermal water samples ranged between − 9.25‰ to − 8.17‰, with an average of − 8.84‰, and the δD ranged from − 73.72‰ to − 69.74‰, with an average of − 71.01‰. Compared with $\delta^{18}O$, the δD of the samples showed significant variation, which caused horizontal drift. For the other groundwater samples, $\delta^{18}O$ ranged between − 8.72‰ to − 8.16‰, with an average of − 8.44‰, and δD ranged between − 68.24‰ to − 65.15‰, with an average of − 66.99‰. Moreover, sample distribution was relatively concentrated, and no drift phenomenon was observed.

Compared with the common groundwater samples, the geothermal water samples had lower values of δD and $\delta^{18}O$, indicating that the geothermal water is possibly recharged from different aquifers than the common groundwater samples. In this study, the scattering of the data points showed that the geothermal water samples were closer to the nearby Ordovician limestone aquifer samples, while the common groundwater samples were closer to the Taiyuan Formation limestone aquifer samples. This agreed with the results from previous studies in the Huaibei coalfield, which reported that the Ordovician limestone aquifer possessed lower values of δD and $\delta^{18}O$ than the Taiyuan Formation limestone aquifer, with typical drift features (Gui et al. 2005; Gui and Chen. 2016). Thus, the Ordovician limestone aquifer is most likely to be the recharge source of the geothermal water and the Taiyuan Formation limestone aquifer is quite likely the recharge source of the common groundwater in the study area.

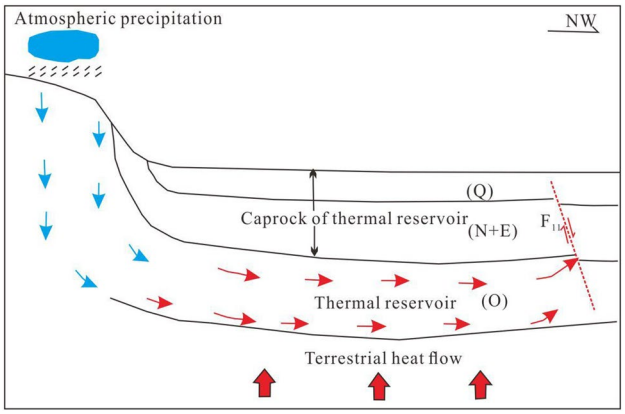

Fig. 7 Schematic diagram of geothermal genesis

Mechanism of Geothermal Water System Formation

The magma chambers melting in the crust and structural faults are the primary heat sources of the geothermal system in the study area (Liu et al. 2020a, b; Zhou et al. 2020; Zucchi 2020). According to the drilling exploration data, no magmatic rocks are exposed in the Qingdong coal mine, and the Huaibei coalfield is situated far from the active plate zone, suggesting that there is no local melting magma chamber in the study area. Fault F_{11}, situated between the geothermal anomaly area and geothermal normal area, serves as a boundary fault and is characterized by a NNE strike, a 45° to 70° dip in a westerly direction, and a drop of > 300 m. The geothermal anomalous area is in the hanging wall of the fault. F_{11} connects the coal mine strata with the Ordovician limestone aquifer, allowing the hot and deep Ordovician limestone aquifer supply to enter the cold and shallow coal mine strata via the water-conducting fault (Gong et al. 2019; Luo et al. 2017), as shown in supplemental Fig. S4.

Since the late Miocene period, the subsidence of the Huaibei Coalfield has been stable, and the Tertiary and Quaternary strata are widely deposited, forming a fine cap rock in the geothermal area, which provides good thermal insulation. The abundant precipitation and surface runoff continuously infiltrate the exposed bedrock and structural fissures, migrating into the thermal reservoir along the rock inter-layer fissures. After a long geological period, the groundwater was heated by deep circulation to form deep geothermal water, and the conducting fault transported the geothermal water into other areas. Figure 7 shows a schematic diagram of the geothermal genesis in the study area. During the convective movement of the geothermal water, the surrounding rock around the fault gradually heats up,

forming an abnormal geothermal area in the Qingdong coal mine. The geothermal water is centrally discharged in the underground mine roadway, resulting in a confined geothermal water system characterized by optimal recharge-runoff-discharge conditions.

We conclude that in the Qingdong coal mine area, convective heat storage is the thermal reservoir mode of the geothermal water; the Ordovician limestone aquifer is the recharge source, and the Ordovician carbonate rock is the thermal reservoir. Moreover, the enrichment and migration of geothermal water is controlled by a water-conducting fault (F_{11}) situated beneath an insulating, thick cap rock.

Conclusions

In this study, the geochemical characteristics and hydrogeochemical processes of geothermal and common groundwater samples obtained from the Qingdong coal mine in China were investigated and compared to determine the chemical composition and formation mechanism of geothermal water in the area. The main conclusions obtained from this study are:

(1) Ca^{2+} and $Na^{+}+K^{+}$ were the most abundant cations in the geothermal water samples, followed by Mg^{2+}. The concentrations of anions in the geothermal water followed the order $SO_4^{2-}>Cl^{-}>HCO3^{-}$. The hydrochemical facies of the geothermal water was 92% SO_4·Cl–Ca.Mg, and 8% SO_4·Cl–Na. Moreover, the high content of TDS, Ca^{2+}, and SO_4^{2-}, and the low concentrations of $Na^{+}+K^{+}$ and HCO_3^{-} are due to the dissolution of minerals and water–rock interactions.

(2) The chemical composition of the geothermal water is controlled by both ion-exchange interactions and dissolution of carbonates and silicates. Moreover, the runoff of common groundwater in the study area is relatively slow, whereas geothermal water possesses optimal hydrodynamic conditions and strong water–rock interactions.

(3) The data points of the geothermal and common groundwater samples plotted in the lower portion of the GMWL, suggesting that precipitation is the primary source of these waters. Moreover, the geothermal water samples had lower δD and $\delta^{18}O$ values, and δD drift in the horizontal direction was observed. Overall, the Ordovician and Taiyuan limestone aquifers were identified as the recharge sources of the geothermal water and common groundwater, respectively.

(4) In the study area, the heat source of the geothermal system is predominately structural faults and not magma chambers melting in the crust. The confined geothermal water in the study area is a convective-type system with tertiary and Quaternary strata forming cap rocks and Ordovician carbonate serving as the reservoir. Moreover, the migration of geothermal water is controlled by a water-conducting fault (F_{11}) located beneath an insulating cap rock.

Supplementary Information The online version contains supplementary material available at https://doi.org/10.1007/s10230-022-00895-2.

Acknowledgements This research was funded by the key scientific research projects of Anhui Provincial Department of Education (KJ2021A1117), the key natural science research projects of Suzhou University (2020yzd03), National Natural Science Foundation of China (41773100), funding projects for research activities of academic and technological leaders of Anhui Province (2020D239), and the Centre for Basic Geology-Suzhou university scientific Centre(2021XJPT55). We also thank Editage (www.editage.cn) for English language editing.

References

Alçiçek H, Bülbül A, Yavuzer İ, Cihat Alçiçek M (2019) Origin and evolution of the thermal waters from the Pamukkale geothermal field (Denizli Basin, SW Anatolia, Turkey): insights from hydrogeochemistry and geothermometry. J Volcanol Geotherm Res 372:48–70. https://doi.org/10.1016/j.jvolgeores.2018.09.011

Chen S, Gui HR (2017) Hydrogeochemical characteristics of groundwater in the coal-bearing aquifer of the Wugou coal mine, northern Anhui Province. China Appl Water Sci 7(4):1903–1910. https://doi.org/10.1007/s13201-015-0365-0

Chen K, Sun LH (2019) Analysis of chemical composition and control factors of groundwater in Renlou coal mine. Coal Sci Technol 47(10):240–244. https://doi.org/10.13199/j.cnki.cst.2019.10.032

Chen MX, Wang J, Deng X (1995) Advances in geothermics in China. J China Univ Geosci 04:367–372

Chen ZX, Cheng J, Guo PW, Lin ZY, Zhang FY (2010) Distribution characteristics and its control factors of stable isotopes in precipitation over China. J Atmos Sci 33(06):667–679. https://doi.org/10.13878/j.cnki.dqkxxb.2010.06.015

Chen LW, Yin XX, Xie WP, Feng XQ (2014) Calculating groundwater mixing ratios in groundwater-inrushing aquifers based on environmental stable isotopes (D, O) and hydrogeochemistry. Nat Hazards 71(1):937–953. https://doi.org/10.1007/s11069-013-0941-2

Chen LW, Xu DQ, Yin XX, Xie WP, Zeng W (2017) Analysis on hydrochemistry and its control factors in the concealed coal mining area in north China: a case study of dominant inrush aquifers in Suxian mining area. J China Coal Soc 42(04):996–1004. https://doi.org/10.13225/j.cnki.jccs.2016.0685

Chen JY, Xu TF, Jiang ZJ, Feng B, Liang X (2020) Reducing formation damage by artificially controlling the fluid-rock chemical interaction in a double-well geothermal heat production system. Renew Energy 149:455–467. https://doi.org/10.1016/j.renene.2019.12.038

Chenaker H, Houha B, Vincent V (2018) Hydrogeochemistry and geothermometry of thermal water from north-eastern Algeria. Geothermics 75:137–145. https://doi.org/10.1016/j.geothermics.2018.04.009

Craig H (1961) Isotopic variations in meteoric waters. Science 133(3465):1702–1703. https://doi.org/10.1126/science.133.3465.1702

Darma S (2016) Indonesia: vast geothermal potential, modest but growing exploitation. Geothermal Power Generation. Woodhead Publishing, pp 609–643

Erdogdu E (2009) A snapshot of geothermal energy potential and utilization in Turkey. Renew Sust Energ Rev 13(9):2535–2543. https://doi.org/10.1016/j.rser.2009.06.020

Gong X, Hou WJ, Feng DL, Luo QZ, Yang XQ (2019) Modelling early karstification in future limestone geothermal reservoirs by mixing of meteoric water with cross-formational warm water. Geothermics 77:313–326. https://doi.org/10.1016/j.geothermics.2018.10.009

Gu XM, Zhang QL, Cui YL, Shao JL, Xiao YL, Zhang PL, Liu JX (2017) Hydrogeochemistry and genesis analysis of thermal and mineral springs in Arxan, northeastern China. Water 9(1):61. https://doi.org/10.3390/w9010061

Guan LS, Gui HR, Zhao HH, Wang MC, Yu H, Fang HX (2020) Nitrogen source analysis and health risk assessment in goaf water of Kouquangou mining area, Datong, China. Fresenius Environ Bull 29(12):10346–10355

Gui HR, Chen S (2016) Isotopic geochemistry characteristics of groundwater its geological significance in the Sunan mining area. Earth Sci Front 23(03):133–139. https://doi.org/10.13745/j.esf.2016.03.017

Gui HR, Lin ML (2016) Types of water hazards in China coal mines and regional characteristics. Nat Hazards 84(2):1501–1512. https://doi.org/10.1007/s11069-016-2488-5

Gui HR, Chen LW, Song XM (2005) Drift features of oxygen and hydrogen stable isotopes in deep groundwater in mining area of northern Anhui. J Harbin Inst Technol 01:111–114. https://doi.org/10.13878/j.cnki.dqkxxb.2010.06.015

Gui HR, Tong SJ, Qiu WZ, Lin ML (2018) Research on preventive technologies for bed-separation water hazard in China coal mines. Appl Water Sci 8(1):1–11. https://doi.org/10.1007/s13201-018-0667-0

Guo Y, Wei JC, Gui HR, Zhang Z, Hu MC (2020) Evaluation of changes in groundwater quality caused by a water inrush event in Taoyuan coal mine, China. Environ Earth Sci 79(24):1–15. https://doi.org/10.1007/s12665-020-09243-5

Hao CM, Wei Z, Gui HR (2020) Hydrogeochemistry characteristic contrasts between low- and high-antimony in shallow drinkable groundwater at the largest antimony mine in Hunan province China. Appl Geochem. https://doi.org/10.1016/j.apgeochem.2020.104584

Hao CM, Zhang W, Tang JL, Gui HR (2021) Water-rock interaction and stable isotopes (34s, 18o) as geochemocal tracing source of sulfate in abandoned mine water: a case study of the Fengfeng coalfield in north China. Fresenius Environ Bull 30(2):1527–1537

Hou JC, Cao MC, Liu PK (2018) Development and utilization of geothermal energy in China: current practices and future strategies. Renew Energy 125:401–412. https://doi.org/10.1016/j.renene.2018.02.115

Hu YH, Wang XM, Dong ZB, Liu GJ, Wang MH, Liu MC (2015) Groundwater quality at the Huaibei coalfield. China Anal Lett 48(10):1654–1669. https://doi.org/10.1080/00032719.2014.991961

Karaoğlu Ö, Bazargan M, Baba A, Browning J (2019) Thermal fluid circulation around the Karliova triple junction: geochemical features and volcano-tectonic implications (eastern Turkey). Geothermics 81:168–184. https://doi.org/10.1016/j.geothermics.2019.05.003

Karmegam U, Chidambaram S, Prasanna M, Sasidha P, Manikandan S, Johnsonbabu G, Dheivanayaki V, Paramaguru P, Manivannan R, Srinivasamoorthy K, Anandhan P (2011) A study on the mixing proportion in groundwater samples by using Piper diagram and Phreeqc model. Chin J Geochem 30(4):490–495. https://doi.org/10.1007/s11631-011-0533-3

Keesari T, Pant D, Roy A, Sinha UK, Jaryal A, Singh M, Jain SK (2021) Fluoride geochemistry and exposure risk through groundwater sources in northeastern parts of Rajasthan. India Arch Environ Contam Toxicol 80(1):294–307. https://doi.org/10.1007/s00244-020-00794-z

Kim K, Rajmohan N, Kim HJ, Hwang GS, Cho MJ (2004) Assessment of groundwater chemistry in a coastal region (Kunsan, Korea) having complex contaminant sources: a stoichiometric approach. Environ Geol 46(6/7):763–774. https://doi.org/10.1007/s00254-004-1109-x

Liu JR, Song XF, Yuan GF, Sun XM, Liu X, Wang SQ (2009) Characteristics of δ18O in precipitation over eastern monsoon China and the water vapor sources. Chin Sci Bull 54(22):3521–3531. https://doi.org/10.1007/s11434-009-0202-7

Liu ML, He T, Wu QF, Guo QH (2020a) Hydrogeochemistry of geothermal waters from Xiongan new area and its indicating significance. Earth Sci 45(06):2221–2231. https://doi.org/10.3799/dqkx.2019.270

Liu YX, Chen LW, He YD, Wang LT, Zhang J, Chen YF (2020b) Groundwater chemical characteristics and circulation mode in the Suixiao coal-mining district. Q J Eng Geol Hydrogeol 53(2):227–235. https://doi.org/10.1144/qjegh2018-208

Luo L, Pang ZH, Liu JX, Hu SB, Rao S, Li YM, Lu LH (2017) Determining the recharge sources and circulation depth of thermal waters in Xianyang geothermal field in Guanzhong Basin: the controlling role of Weibei fault. Geothermics 69:55–64. https://doi.org/10.1016/j.geothermics.2017.04.006

Nasruddin N, Idrus Alhamid M, Daud Y, Surachman A, Sugiyono A, Aditya HB, Mahlia TMI (2016) Potential of geothermal energy for electricity generation in Indonesia: a review. Renew Sust Energ Rev 53:733–740. https://doi.org/10.1016/j.rser.2015.09.032

Oosawa Y, Kasai M (1988) Gibbs-Donnan ratio and channel conductance of Tetrahymena cilia in mixed solution of K+ and Ca^{2+}. Biophys J 54(3):407–410. https://doi.org/10.1016/S0006-3495(88)82974-6

Prada S, Cruz JV, Figueira C (2016) Using stable isotopes to characterize groundwater recharge sources in the volcanic island of Madeira, Portugal. J Hydrol 536:409–425. https://doi.org/10.1016/j.jhydrol.2016.03.009

Tay C, Kortatsi B, Hayford E, Hodgson I (2014) Origin of major dissolved ions in groundwater within the Lower Pra Basin using groundwater geochemistry, source-rock deduction and stable isotopes of H and O. Environ Earth Sci 71(12):5079–5097. https://doi.org/10.1007/s12665-013-2912-z

Tran TQ, Banning A, Wisotzky F, Wohnlich S (2020) Mine water hydrogeochemistry of abandoned coal mines in the outcropped Carboniferous formations, Ruhr Area. Germany Environ Earth Sci 79(4):1–16. https://doi.org/10.1007/s12665-020-8821-z

Wang H, Jiang XW, Wan L, Han GL, Guo HM (2015) Hydrogeochemical characterization of groundwater flow systems in the discharge area of a river basin. J Hydrol 527:433–441

Wang M, Gui H, Hu R, Zhao H, Li J, Yu H, Fang H (2019) Hydrogeochemical characteristics and water quality evaluation of Carboniferous Taiyuan formation limestone water in Sulin mining area in northern Anhui, China. Int J Environ Res Public Health 16(14):2512–2512. https://doi.org/10.1016/j.jhydrol.2015.04.063

Weiß EG (2020) Renewable geothermal energy – latest developments in geothermics in North Rhine-Westphalia: new finds, new projects, new research facilities. Min Rep 156(6):533–540

Xu PP, Li MN, Qian H, Zhang QY, Liu FX, Hou K (2019) Hydrochemistry and geothermometry of geothermal water in the central Guanzhong Basin, China: a case study in Xi'an. Environ Earth Sci 78(3):1–1. https://doi.org/10.1007/s12665-019-8099-1

Zhang HT, Xu GQ, Chen XQ, Mabaire A (2019a) Hydrogeochemical evolution of multilayer aquifers in a massive

coalfield. Environ Earth Sci 78(24):1–17. https://doi.org/10.1007/s12665-019-8694-1

Zhang HT, Xu GQ, Chen XQ, Wei J, Yu ST, Yang TT (2019b) Hydrogeochemical characteristics and groundwater inrush source identification for a multi-aquifer system in a coal mine. Acta Geol Sin (engl Ed) 93(6):1922–1932. https://doi.org/10.1111/1755-6724.14299

Zhang SC, Shen BT, Li YY, Zhou SF (2019c) Modeling rock fracture propagation and water inrush mechanisms in underground coal mine. Geofluids. https://doi.org/10.1155/2019/1796965

Zhang J, Chen LW, Chen YF, Guo YT, Ma L, Zhou KD, Shi XP (2020a) Discrimination of water-inrush source and evolution analysis of hydrochemical environment under mining in Renlou coal mine, Anhui Province. China Environ Earth Sci 79(2):1–13. https://doi.org/10.1007/s12665-019-8803-1

Zhang LP, Ma BQ, Bin F, Meng H (2020b) Hydrochemical origin and indicative significance of deep geothermal water in Lanzhou City. Water Resour Hydropower Eng 51(08):129–139. https://doi.org/10.13928/j.cnki.wrahe.2020.08.016

Zhou Z, Jin Y, Zeng YJ, Zhang XD, Zhou J, Zhuang L, Xin SY (2020) Investigation on fracture creation in hot dry rock geothermal formations of China during hydraulic fracturing. Renew Energy 153:301–313. https://doi.org/10.1016/j.renene.2020.01.128

Zucchi M (2020) Faults controlling geothermal fluid flow in low permeability rock volumes: An example from the exhumed geothermal system of eastern Elba Island (northern Tyrrhenian Sea Italy). Geothermics. https://doi.org/10.1016/j.geothermics.2019.101765